

Transport Properties of Strongly Correlated Fermi Systems

Vasily R. Shaginyan ^{1,2,*} , Alfred Z. Msezane ^{2,*}  and Mikhail V. Zverev ^{3,4}¹ Petersburg Nuclear Physics Institute, NRC Kurchatov Institute, Gatchina 188300, Russia² Department of Physics, Clark Atlanta University, Atlanta, GA 30314, USA³ NRC Kurchatov Institute, Moscow 123182, Russia; zverev.mv@phystech.edu⁴ Department of Physical and Quantum Electronics, Moscow Institute of Physics and Technology, Moscow 141700, Russia

* Correspondence: vrshag@thd.pnpi.spb.ru (V.R.S.); amsezane@cau.edu (A.Z.M.)

Abstract: Physicists are actively debating the nature of the quantum critical phase transition that determines the low-temperature properties of metals with heavy fermions. Important experimental observations of their transport properties incisively probe the nature of the quantum critical phase transition. In our short review, we consider the transport properties of strongly correlated Fermi systems like heavy fermion metals and high- T_c superconductors. Their transport properties are defined by strong inter-particle interactions, forming flat bands in these compounds. These properties do not coincide with those of conventional metals. Indeed, in contrast to the behavior of the transport properties of conventional metals, the strongly correlated compounds exhibit linear temperature resistivity $\rho(T) \propto T$. We analyze the magnetoresistance and show that under the application of the magnetic field, it becomes negative. It is shown that near a quantum phase transition, when the density of the electronic states diverges, semiclassical physics remains applicable to describe the resistivity ρ of strongly correlated metals due to the presence of a transverse zero-sound collective mode, representing the phonon mode in solids. We demonstrate that when T exceeds the extremely low Debye temperature T_D , the resistivity $\rho(T)$ changes linearly with T since the mechanism of formation of the T -dependence $\rho(T)$ is a similar electron-phonon mechanism, which predominates at high temperatures in ordinary metals. Thus, in the region of T -linear resistance, electron-phonon scattering leads to a lifetime of τ quasiparticles practically independent of the material, which is expressed as the ratio of the Planck constant \hbar to the Boltzmann constant k_B , $T\tau \sim \hbar/k_B$. We explain that due to the non-Fermi-liquid behavior, the real part of the frequency-dependent optical conductivity $\sigma_{opt}^R(\omega)$ exhibits a scaling behavior and demonstrates the unusual power law behavior $\sigma_{opt}^R(\omega) \propto \omega^{-1}$, rather than the well-known one shown by conventional metals, $\sigma_{opt}^R(\omega) \propto \omega^{-2}$. All our theoretical considerations are illustrated and compared with the corresponding experimental facts. Our results are in a good agreement with experimental observations.

Keywords: quantum phase transitions; heavy fermions; non-Fermi liquid behavior; scaling behavior; topological phase transitions



Citation: Shaginyan, V.R.; Msezane, A.Z.; Zverev, M.V. Transport Properties of Strongly Correlated Fermi Systems. *Symmetry* **2023**, *15*, 2055. <https://doi.org/10.3390/sym15112055>

Academic Editors: Vyacheslav Yukalov, V. S. Bagnato and Rashid G. Nazmitdinov

Received: 17 September 2023

Revised: 11 October 2023

Accepted: 2 November 2023

Published: 13 November 2023



Copyright: © 2023 by the authors. Licensee MDPI, Basel, Switzerland. This article is an open access article distributed under the terms and conditions of the Creative Commons Attribution (CC BY) license (<https://creativecommons.org/licenses/by/4.0/>).

1. Introduction

An explanation of the rich and striking behavior of a strongly correlated electron liquid in heavy fermion (HF) metals, high-temperature superconductors, quasicrystals, etc., is among the main problems of condensed matter physics. Quantum phase transitions (QPTs) define the non-Fermi liquid (NFL) low-temperature properties of strongly correlated Fermi systems. Their behavior in the NFL state is so radical that the traditional quasiparticle Landau paradigm cannot describe it. The underlying nature of QPT continues to challenge theoretical understanding. Attempts have been made to use concepts such as the Kondo lattice and quantum and thermal fluctuations in QPT [1–5]. Alas, when these approaches are designed to describe one property that is considered central, they cannot explain others, even the simplest ones, such as the Kadowaki-Woods relation [6,7]. This relationship, which

naturally arises with the leading role of quasiparticles of the effective mass M^* , can hardly be explained within the framework of a theory that assumes the absence of quasiparticles; see [7–10]. Arguments that quasiparticles in strongly correlated Fermi liquids become heavy and die during QPT are usually based on the assumption that the quasiparticle weight factor Z vanishes at the point of the corresponding second-order phase transition [11,12]. However, this scenario does not correspond to experimental facts [7,13,14]. Numerous experimental facts have been discussed within the framework of such a concept, but how it can quantitatively explain the physics of HF metals remains an open question. The theory of fermion condensation was proposed and developed, preserving quasiparticles. The fermion condensation (FC) takes place at the topological fermion condensation quantum phase transition (FCQPT), and leads to both flat bands, which was predicted in 1990 [15], and to the unlimited growth of the effective mass M^* ; at the same time, the extensive research has shown that this theory provides an adequate theoretical explanation for the vast majority of experimental results with various HF metals [7–10,15–22]. Unlike the Landau paradigm, which is based on the assumption that M^* is approximately constant, in the FC theory, M^* strongly depends on temperature T , applied magnetic field B , etc. It is important to note that the extended quasiparticle paradigm has been introduced. The essential point is that, as before, well-defined quasiparticles determine the thermodynamic and transport properties of strongly correlated Fermi systems [7]. Indeed, the width of quasiparticles tends to zero at $T \rightarrow 0$, and they are well-defined excitations up to $T \sim 100$ K [7,23]. In fact, this observation is in accordance with numerous experimental observations; for example, the typical behavior of the heat capacity of HF metals defined by quasiparticles is observed in a wide range of temperatures; see [7]. The dependence of the effective mass M^* on T and B leads to both the observed NFL behavior and the restoration of the Landau Fermi liquid behavior at low temperatures under the application of magnetic fields [7–10]. The most fruitful strategy for studying and uncovering the nature of QPT is to focus on those properties that exhibit the most dramatic deviations from the Landau Fermi liquid (LFL) behavior of ordinary metals at low temperatures [24–26].

In our review, we consider the transport properties that allow one to disclose the nature of QPT governing the behavior HF metals. In particular, measurements of the magnetoresistance clarifies the dependence of the effective mass M^* on applied magnetic field B since, in contrast to ordinary metals, the magnetoresistance becomes negative under the application of B ; see [27–29]. This point is considered in Sections 2 and 3. Relationships between the NFL resistivity $\rho(T) \propto T$ and the so-called Planckian limit open new possibilities to analyze the properties of QPT that govern the transport properties of HF metals [30,31]; see Sections 4 and 5. Precise experimental measurements of the optical conductivity of HF metals YbRh_2Si_2 and $\text{La}_{2-x}\text{Sr}_x\text{CuO}_4$ have been carried out (see [32,33]), which probe the nature of their QPT. It was discovered that at low temperatures, the optical conductivity is very different from the well-known optical conductivity of ordinary metals [32,33]; see Sections 4 and 6. In Section 2, we consider general properties of the effective mass M^* in magnetic fields. Section 7 is devoted to the main conclusion of our review.

2. The Behavior of the Effective Mass

We start with analyzing the scaling behavior of the effective mass M^* and the schematic T - B phase diagram of HF metals based on the homogeneous HF liquid, thereby avoiding complications associated with the crystalline anisotropy of solids [7,9]. Before the topological FCQPT, the temperature and magnetic field dependencies of the effective mass $M^*(T, B)$ were governed by the Landau equation [24–26]:

$$\frac{1}{M_\sigma^*(T, B)} = \frac{1}{m} + \sum_{\sigma_1} \int \frac{\mathbf{p}_F \mathbf{p}}{p_F^3} F_{\sigma, \sigma_1}(\mathbf{p}_F, \mathbf{p}) \times \frac{\partial n_{\sigma_1}(\mathbf{p}, T, B)}{\partial p} \frac{dp}{(2\pi)^3}. \quad (1)$$

where $F_{\sigma,\sigma_1}(\mathbf{p}_F, \mathbf{p})$ is the Landau interaction, p_F is the Fermi momentum, and σ is the spin label. We note that Equation (1) is an exact one, as it can be shown within the framework of the Density Function Theory; see [7,9,34]. To simplify matters, we ignore the spin dependence of the effective mass, noting that $M^*(T, B)$ is nearly independent of spin in weak fields. The quasiparticle distribution function $n(\mathbf{p}, T)$ is given by

$$n_{\sigma}(\mathbf{p}, T) = \left\{ 1 + \exp \left[\frac{(\varepsilon(\mathbf{p}, T) - \mu_{\sigma})}{T} \right] \right\}^{-1}, \quad (2)$$

where $\varepsilon(\mathbf{p}, T)$ is the single-particle spectrum. In the case being considered, the spectrum depends on spin only weakly. However, the chemical potential μ_{σ} depends non-trivially on spin due to the Zeeman splitting, $\mu_{\pm} = \mu \pm B\mu_B$, where \pm corresponds to states with the spin “up” or “down.” Numerical and analytical solutions of this equation show that the dependence of the effective mass $M^*(T, B)$ on the temperature T and magnetic field B leads to the appearance of three different regimes with increasing temperature. The Fermi-Dirac distribution function can be presented as follows:

$$\varepsilon(\mathbf{p}) - \mu = T \ln \frac{1 - n(\mathbf{p})}{n(\mathbf{p})}, \quad (3)$$

where μ is the chemical potential, and $n(\mathbf{p})$ is the quasiparticle occupation number. In the theory of fermion condensation, if the system is located near the topological FCQPT on its ordered side, the quasiparticle occupation number loses its temperature dependence at sufficiently low T [7,15,23]. In the interval $p_i \leq p \leq p_f$, the quasiparticle distribution function $n(\mathbf{p}) < 1$; therefore, the logarithm in Equation (3) is finite, and at $T = 0$, the product on the right-hand side of Equation (3) is zero. As a result, on the ordered side of the topological FCQPT, the spectrum contains a flat band [7,15,23]:

$$\varepsilon(\mathbf{p}) - \mu = 0 \text{ if } p_i \leq p \leq p_f. \quad (4)$$

The existence of the solution of Equation (4) means that the single-particle spectrum $\varepsilon(\mathbf{p}, T)$ has a flat band. Since $\varepsilon(\mathbf{p}) = \mu$ in the range $p_i \leq p \leq p_f$, the Fermi surface spreads into a Fermi band, that is, in the case of the three-dimensional Fermi sphere, the two-dimensional Fermi surface transforms into a three-dimensional structure. Obviously, this transformation gives rise to a change in the topological structure of the single particle Green function, which makes us refer to the systems with FC as a new class of Fermi liquids being different from both the Landau Fermi liquid [24] and the marginal Fermi liquid (see [35]) and with its specific topological charge [16,19]. We note that Equations (3) and (4) are exact; see [7,9,34].

It is seen from Equation (3) that at any finite temperature, the flat band given by Equation (4) vanishes, and the effective mass becomes finite [7,36]. On the disordered side, at finite B and sufficiently low temperatures T , we have the LFL state with $M^*(T) \simeq M^* + aT^2$, where a is a positive constant. Thus, the effective mass grows as a function of T , reaching a maximum M_M^* at a certain temperature T_M and then decreasing (see, for example, [7,36,37]):

$$M^*(T) \propto T^{-2/3}. \quad (5)$$

The application of magnetic field restores the LFL behavior, and at $T \leq T_M$, the effective mass depends on B as [7]

$$M^*(B) \propto (B - B_{c0})^{-2/3}, \quad (6)$$

as it is seen from Figure 1.

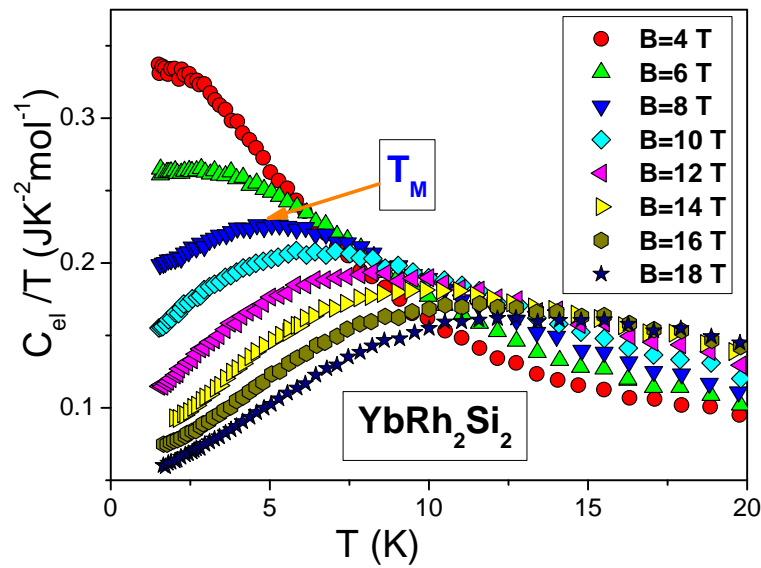


Figure 1. Electronic heat capacity YbRh_2Si_2 , C_{el}/T , as a function of temperature T and as a function of magnetic field B [37], shown in the legend. As an example, the maximum value M_M taking place at T_M and $B = 8$ T is shown by the arrow.

Note that in some cases, the critical magnetic field B_{c0} that tunes HF metal to its FCQPT can be zero, $B_{c0} = 0$. For instance, the HF metal CeRu_2Si_2 is characterized by $B_{c0} = 0$ and shows no signs of magnetic ordering, superconductivity, or the LFL behavior down to the lowest temperatures [38]. Moreover, the closer the control parameter B is to its critical value $B_{c0} = 0$, the higher the growth rate. In this case, the peak value of M_M^* also increases, but the temperature T_M , at which M^* reaches its maximum value, decreases, and $M_M^*(T_M, B \rightarrow B_{c0}) \rightarrow \infty$. At $T > T_M$, the LFL behavior disappears. When the system is near FCQPT, the approximate interpolation solution to the Equation (1) has the form [7]

$$\frac{M^*}{M_M^*} = M_N^*(T_N) \approx c_0 \frac{1 + c_1 T_N^2}{1 + c_2 T_N^{8/3}}. \quad (7)$$

Here, $T_N = T/T_M$ is the normalized temperature, with $c_0 = (1 + c_2)/(1 + c_1)$ in terms of fitting parameters c_1 and c_2 . Since the magnetic field enters Equation (2) in the form $\mu_B B/T$, we conclude that

$$T/T_M = T_N \propto \frac{T}{\mu_B B}, \quad (8)$$

where μ_B is the Bohr magneton. It follows from Equation (8) that

$$T_M \simeq a_1 \mu_B B. \quad (9)$$

As a result, we conclude from Equations (8) and (9) that $M_N(y)$ exhibits the scaling behavior as a function of both the variables $y = T/B$ and $y = B/T$. Equation (7) reveals the scaling behavior of the normalized effective mass $M_N^*(T_N = y)$: Values of the effective mass $M^*(T, B)$ at different magnetic fields B merge into a single mass value M_N^* in terms of the normalized variable $T_N \propto T/B \propto B/T$ [7,9]. Figure 2 demonstrates the scaling behavior of the normalized effective mass M_N^* versus the normalized temperature T_N . The LFL phase prevails at $T \ll T_M$, followed by the $T^{-2/3}$ regime at $T \gtrsim T_M$. The latter phase is designated as NFL due to the strong dependence of the effective mass on temperature. The temperature region $T \simeq T_M$ covers the transition between the LFL regime with almost constant effective mass and the LPL behavior described by the Equation (5). Thus, $T \sim T_M$ defines a transition region characterized by the intersection of the LFL and NFL regimes. The inflection point T_{inf} of M_N^* versus T_N is depicted by arrows in Figure 2.

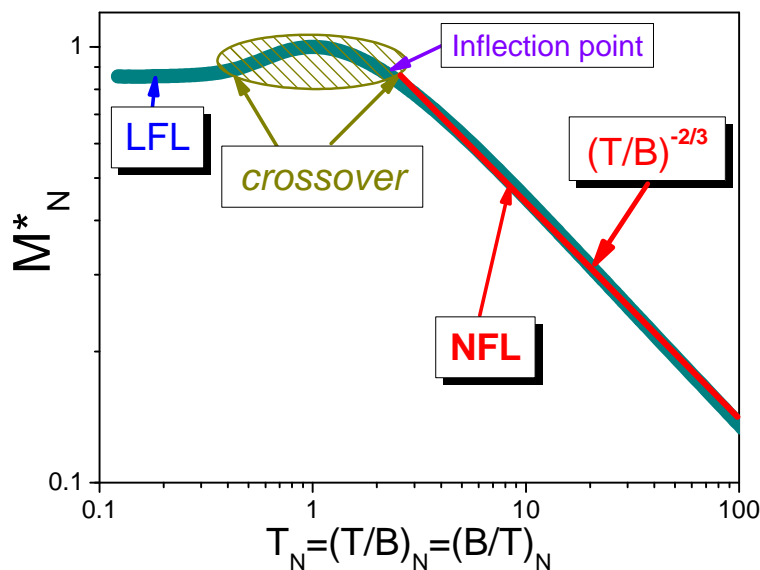


Figure 2. The schematic plot of the normalized effective mass versus the normalized temperature. The transition regime, where M_N^* reaches its maximum value at $T_N = T/T_M = (T/B)_N = (B/T)_N = 1$, is shown as the hatched area. Arrows indicate the LFL region, transition one, inflection point T_{inf} and NFL behavior with $M_N^* \propto (T/B)^{-2/3}$.

The transition (crossover) temperature $T_M(B)$ is not actually the temperature of a phase transition. Its specification is necessarily ambiguous because it depends on the criteria used to determine the point the crossover. Typically, the temperature $T^*(B)$ is obtained from the field dependence of the charge transfer, for example, from the resistivity $\rho(T)$, determined by the expression

$$\rho(T) = \rho_0 + AT^\beta, \tag{10}$$

where ρ_0 is the residual resistivity, and A is a T -independent coefficient. The term ρ_0 is ordinarily attributed to impurity scattering. The LFL state is characterized by the T^β dependence of the resistivity with index $\beta = 2$. The schematic phase diagram of a HF metal is depicted in Figure 3, with the magnetic field B serving as the control parameter. The crossover (through the transition regime shown as the hatched area in Figure 3) takes place at temperatures where the resistance starts to deviate from LFL behavior, with the exponent β shifting from 2 into the range $1 < \beta < 2$. At $B = 0$, the HF metal acquires a flat band corresponding to a strongly degenerate state.

The NFL mode reigns at elevated temperatures and a fixed magnetic field. As B increases, the system moves from the NFL region to the LFL domain. As shown in Figure 3, the system moves from the NFL mode to the LFL mode by the horizontal arrow, and from the LFL mode to the NFL mode by the vertical arrow. The magnetic field tuned QCP is indicated by an arrow and is located at the beginning of the phase diagram since the application of a magnetic field destroys the flat band and transfers the system to the LFL state [7–10]. The shaded area, denoting the transition region, separates the NFL state from the weakly polarized LFL state and contains the dashed line displaying $T_M(B)$. Referring to Equation (9), this line is defined by $T = a_1\mu_B B$. It is worth noting that the transition from the NFL behavior to the LFL taking place under the application of the magnetic field, as it is seen in Figures 2 and 3, is the special property of the topological FCQPT and described by Equation (7) [7,39]. This important property is in a good agreement with experimental facts and allows one to use it as the versatile tool to explore the physics of HF compounds, including the violation of both the particle-hole symmetry and the time invariance symmetry; this violation is directly related to the concept of flat bands [7,40], see

Sections 5 and 6. In contrast, these properties are not considered in a number of theories, including the theory of marginal Fermi liquid, see e.g., [35].

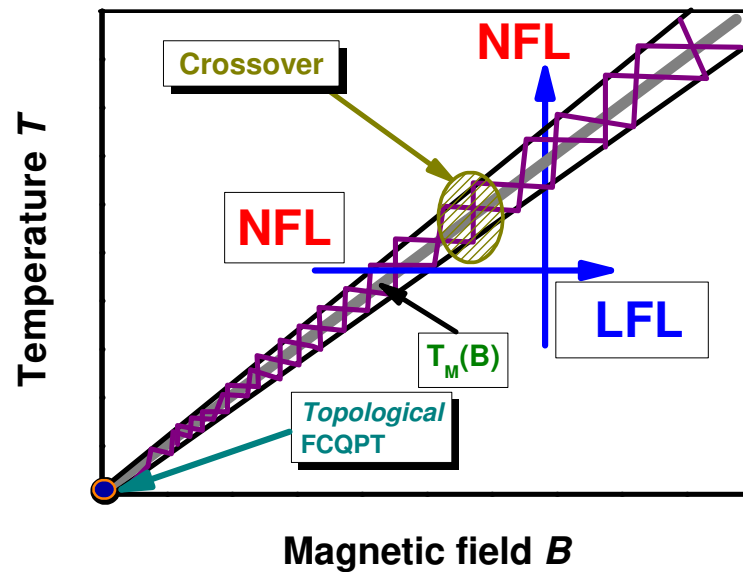


Figure 3. Schematic T - B phase diagram of a HF compound, with magnetic field B as control parameter. The hatched area corresponds to the crossover domain at $T_M(B)$. At a fixed magnetic field and elevated temperature (vertical arrow), there is a LFL-NFL crossover. The horizontal arrow indicates a NFL-LFL transition at a fixed temperature and elevated magnetic field. The topological FCQPT (shown by the arrow) occurs at $T = 0$ and $B = 0$.

3. Longitudinal Magnetoresistance

Consider longitudinal magnetoresistance (LMR)

$$\rho(B, T) = \rho_0 + A(B)T^2, \quad (11)$$

as a function of B at fixed T . In this case, the classical contribution to LMR formed by the orbital motion of carriers induced by the Lorentz force is small. In the LFL state, the Kadowaki-Woods relation is given by [6,7]

$$K = A/\gamma_0^2 \propto A/\chi^2 = const, \quad (12)$$

which allows us to employ M^* to construct the coefficient A since $\gamma_0 \propto \chi \propto M^*$. Here, γ_0 is the Sommerfeld coefficient, and χ is the magnetic susceptibility. Omitting the classical contribution to LMR, we obtain that $\rho(B, T) - \rho_0 \propto (M^*)^2$ [39]. The magnetic field dependence of the muon spin-lattice relaxation rate $1/T_1^\mu$ is given by [39,41]

$$\frac{1}{T_1^\mu T} = \eta[M^*(T, B)]^2, \quad (13)$$

where η is a constant. We note here that the experimentally observed relation

$$\frac{1}{T_1^\mu T} \propto \chi^2 \quad (14)$$

follows explicitly from Equations (12) and (13) [39]. Figure 4 shows the normalized values of both the magnetoresistance of YbRh_2Si_2 [28,29]

$$\rho_N(B_N) = (M_N^*(B_N))^2 \quad (15)$$

and the muon spin-lattice relaxation rate of $\text{YbCu}_{5-x}\text{Au}_x$ ($x = 0.6$) [41]

$$\left(\frac{1}{T_1^\mu T}\right)_N = (M_N^*(B_N))^2 \tag{16}$$

versus normalized magnetic field $B_N = B/B_{inf}$ at different temperatures, shown in the legend. It is seen from Equations (6), (15) and (16) that both LMR and the the muon spin-lattice relaxation rate are diminishing functions of magnetic field B . This result is the vivid feature of the fermion condensation theory that allows one to evaluate the behavior of the effective mass under the application of magnetic fields; see [7,40].

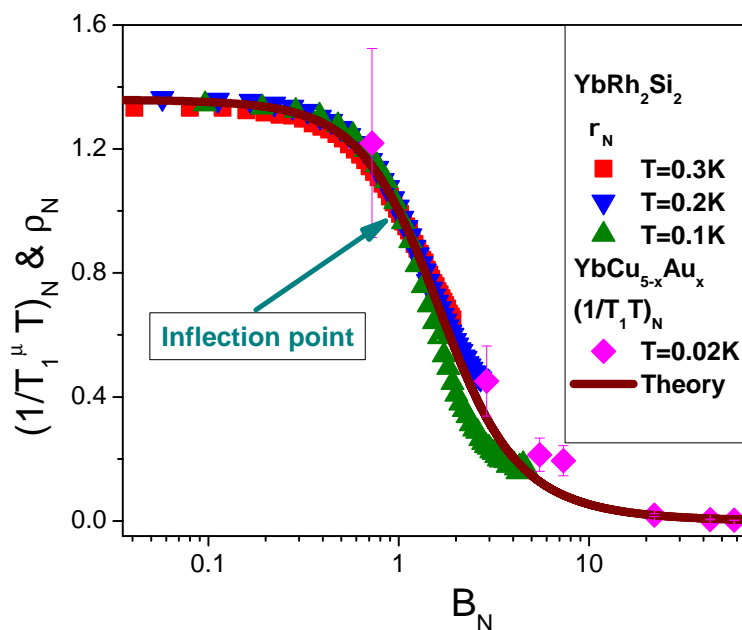


Figure 4. Magnetic field dependence of both the normalized magnetoresistance ρ_N and the muon spin-lattice relaxation rate $(1/T_1^\mu T)_N$ versus normalized magnetic field B_N . ρ_N was extracted from the LMR of YbRh_2Si_2 at different temperatures [28,29] listed in the legend. Magnetic field dependence of normalized muon spin-lattice relaxation rate $1/T_1^\mu T$ in $\text{YbCu}_{4.4}\text{Au}_{0.6}$ is shown by diamonds and extracted from [41]. The data are normalized in the inflection point and shown by the arrow. The solid line represents our calculations; see Equations (6), (15) and (16).

The normalization procedure deserves a remark here. Namely, since the magnetic field dependence (both theoretical and experimental) of $1/T_1^\mu T$ and LMR do not have “peculiar points” like extrema, the normalization is performed in the inflection point, corresponding to the maximum of the corresponding derivative. It is seen that such a procedure immediately reveals the universal magnetic field behavior of both the reciprocal relaxation time and LMR, showing their proportionality to the effective mass square; see Equations (15) and (16). This behavior obtained directly from the experimental findings is vivid evidence that the above quantities’ behavior is predominantly governed by the field B and temperature T dependence of the effective mass $M^*(B, T)$ given by Equation (7). We note that the entire field (and temperature) dependence of both $1/T_1^\mu T$ and LMR is completely determined by the corresponding dependence of the effective mass M_N^* shown in Figure 2. The fact that the effective mass becomes field B , temperature T and the other external dependent parameters is the key consequence of the FC theory. Both the theoretical curve and the experimental data are normalized by their inflection points, which also reveal the universal scaling behavior: the curves at different temperatures merge into a single one in terms of scaled variable B_N . Figure 4 shows clearly that both the normalized magnetoresistance ρ_N and the muon spin-lattice relaxation rate time $1/T_1^\mu T$ well obey the scaling behavior given by Equations (7), (15) and (16) and shown in Figure 2.

4. Linear in Temperature Resistivity

To analyze the resistivity given by Equation (10) at elevated temperatures T and under the application of magnetic field B , we assume that the electron system of the HF metal contains a flat band. The flattening of the single-particle spectrum $\varepsilon(\mathbf{p})$ is directly related to the problem being solved, since as a result of Umklapp processes, quasiparticles of the flat band create a contribution to ρ_0 indistinguishable from the contribution due to the scattering of impurities [42]. Furthermore, it is crucial that the flat band somehow becomes destroyed at $T \rightarrow 0$, and under the application of a magnetic field, the HF metal transits to the LFL state; see Figure 3. This destruction entails a strong suppression of the flat band contribution to ρ_0 [42]. Before proceeding to the analysis of this destruction, we pay attention to the vivid consequences of the flattening of $\varepsilon(\mathbf{p})$ in strongly correlated Fermi systems. The theoretical possibility of this phenomenon and its consequences, also called swelling of the Fermi surface or the fermion condensation, was discovered a few decades ago [15,16,43]; for recent reviews; see [7–10]. At $T = 0$, the ground state of the flat band system is degenerate, and so the occupation number $n_0(\mathbf{p})$ of single-particle states belonging to the flat band forming the fermion condensate are continuous functions of momentum that interpolate between standard LFL values $\{0, 1\}$ in the area occupied by FC; see Equation (4). This leads to an entropy excess

$$S_0 = - \sum_{\mathbf{p}} n_0(\mathbf{p}) \ln n_0(\mathbf{p}) + (1 - n_0(\mathbf{p})) \ln(1 - n_0(\mathbf{p})), \quad (17)$$

which does not contribute to the specific heat $C(T)$. It is seen from Equation (17) that in contrast to the corresponding LFL entropy vanishing linearly as $T \rightarrow 0$, the entropy of the system with the fermion condensates $S(T \rightarrow 0) \rightarrow S_0$. In the theory of fermion condensation, the aforementioned ground-state degeneracy is lifted at any finite temperature, where FC acquires a small dispersion proportional to T ; see Equation (3). However, the removal of degeneracy with increasing temperature does not change the occupation number $n_0(\mathbf{p})$, which means that the excess entropy S_0 will persist down to zero temperature. To avoid a subsequent violation of Nernst's theorem, it is necessary to completely eliminate FC at $T \rightarrow 0$. In the most natural scenario, this occurs through a SC phase transition, in which FC is destroyed with the appearance of a Δ pairing gap in the single-particle spectrum [7,15,23]. We assume that this scenario is realized in CeCoIn₅ at sufficiently weak magnetic fields, ensuring the elimination of the flat portion in the spectrum $\varepsilon(\mathbf{p})$ and the removal of excess entropy S_0 [42]. In stronger external magnetic fields B sufficient to terminate superconductivity in CeCoIn₅, this path becomes ineffective, giving way to an alternative scenario involving a transition from the FC state to the LFL state with a multiply connected Fermi surface [7]. In the phase diagram depicted in Figure 3, such a crossover is indicated by the hatched area between the domains of NFL and LFL behavior and also by the line $T_M(B)$. In case of the HF metal CeCoIn₅, the end point of the curve $T_M(B)$ nominally separating the NFL and LFL phases is the magnetic field inducing the topological FCQPT hidden in the SC state [42,44,45]. This is the most characteristic feature of the phase diagram of the behavior of resistivity $\rho(T, B)$. Since the entropies of the two phases are different, near the topological FCQPT, the SC transition should become of the first order [7], which is consistent with the experimental fact [46]. Moreover, under the application of sufficiently high magnetic field B , the LFL behavior remains in effect even to $T \rightarrow 0$. Thus, the imposition of magnetic field B drives the system in question from its SC phase to the LFL phase. As a result, the FC state or, equivalently, the flat portion of the spectrum $\varepsilon(\mathbf{p})$ is destroyed. Thus, application of a high magnetic field to CeCoIn₅ causes a step-like drop in its residual resistivity ρ_0 , as it is seen experimentally [27]. In addition, it should be expected that the higher the quality of the CeCoIn₅ single crystal, the stronger the suppression of ρ_0 . Now we consider the low-temperature transport properties of the normal state of CeCoIn₅. We use a two-band model, one of which is assumed to be flat with dispersion given by Equation (3), and the second band is assumed to have a single-particle LFL spectrum with finite T -independent dispersion [42].

We begin our consideration with the case when a HF metal is in its normal state, where the resistivity is a linear function of T . This behavior is inherent in electronic systems with flat bands. Now, we define the conductivity $\sigma(T)$ in terms of the imaginary part of the polarization operator $\Pi(\mathbf{j})$ [26],

$$\begin{aligned} \sigma &= \lim \omega^{-1} \text{Im} \Pi(\mathbf{j}, \omega \rightarrow 0) \propto \frac{1}{T} \int \int \frac{dv d\epsilon}{\cosh^2(\epsilon/2T)} \\ &\times |\mathcal{T}(\mathbf{j}, \omega = 0)|^2 \text{Im} G_R(\mathbf{p}, \epsilon) \text{Im} G_R(\mathbf{p}, \epsilon), \end{aligned} \quad (18)$$

where dv is an element of momentum space, $\mathcal{T}(\mathbf{j}, \omega)$ is the vertex part, \mathbf{j} is the electric current, and $G_R(\mathbf{p}, \epsilon)$ is the retarded quasiparticle Green function. The imaginary part reads

$$\text{Im} G_R(\mathbf{p}, \epsilon) = -\frac{\gamma}{(\epsilon - \epsilon(\mathbf{p}))^2 + \gamma^2} \quad (19)$$

in terms of the spectrum $\epsilon(\mathbf{p})$ and the damping γ related to the band with a finite value v_F of the Fermi velocity. Applying gauge invariance, we obtain $\mathcal{T}(\mathbf{j}, \omega = 0) = e \partial \epsilon(\mathbf{p}) / \partial \mathbf{p}$. Substituting this equation into Equation (18) and performing some algebra, we arrive at the standard result

$$\sigma(T) = e^2 n \frac{v_F}{\gamma(T)}, \quad (20)$$

where n is the number density of electrons.

In ordinary pure metals obeying the LFL theory, the damping $\gamma(T)$ is proportional to T^2 , which leads to Equation (10) with $\beta = 2$. The NFL behavior of $\sigma(T)$ is due to the NFL dependence of $\gamma(T)$ on the temperature associated with the presence of FC [42]. In a standard situation, when the volume η occupied by FC is quite small, the overwhelming contribution to the transport is made by inelastic scattering, schematically presented in Figure 5a,b, where FC quasiparticles (highlighted by a double line) turn into normal quasiparticles, or vice versa, normal quasiparticles rotate into FC quasiparticles. The contributions of these processes to damping γ are estimated based on the simplified equation [26]:

$$\begin{aligned} \gamma(\mathbf{p}, \epsilon) &\propto \int \int \int_0^\epsilon \int_0^\omega |\Gamma(\mathbf{p}, \mathbf{p}_1, \mathbf{q})|^2 \text{Im} G_R(\mathbf{p} - \mathbf{q}, \epsilon - \omega) \\ &\times \text{Im} G_R(-\mathbf{p}_1, -\epsilon) \text{Im} G_R(\mathbf{q} - \mathbf{p}_1, \omega - \epsilon) d\mathbf{p}_1 d\mathbf{q} d\omega d\epsilon, \end{aligned} \quad (21)$$

where, now, the volume element in momentum space includes summation over different bands. The straightforward calculations give:

$$\gamma(\epsilon) = \eta(\gamma_0 + \gamma_1 \epsilon), \quad \text{Re} \Sigma(\epsilon) = -\eta \gamma_1 \epsilon \ln \frac{\epsilon_c}{|\epsilon|}, \quad (22)$$

where η denotes the volume of momentum space occupied by the flat band, and ϵ_c is the characteristic constant defining the logarithmic term in Σ . Taking vertex corrections into account [26] provides transparent changes to Equation (21) and cannot be held responsible for the effects discussed here.

Note that Equation (33) gives the lifetime τ of quasiparticles,

$$\hbar/\tau = \gamma(T) \simeq a_0 + a_1 T, \quad (23)$$

where \hbar is Planck's constant, and a_0 and a_1 are parameters. Combining Equations (22) and (23), we obtain

$$\hbar/\tau(\epsilon, T) = \gamma(\epsilon, T) \simeq a_0 + a_1 T + a_2 \epsilon. \quad (24)$$

where $a_0 \propto \rho_0$, a_1 and a_2 are parameters. This result is in good agreement with the experimental facts [47,48], as it is seen from Figure 6. Considering Equation (23), one immediately sees that $\rho(T) = \rho_0 + AT$, i.e., the resistivity $\rho(T)$ of systems containing FC, is

indeed a linear function of T , which is consistent with the experimental data collected on CeCoIn_5 ; see Figure 6. Moreover, the ρ_0 term appears even if the metal has an ideal lattice and no impurities at all.

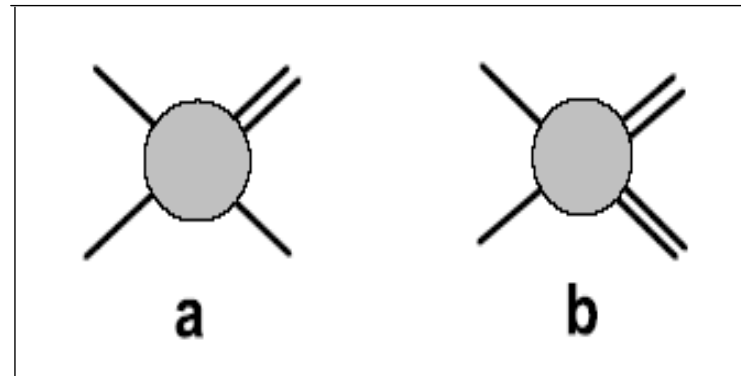


Figure 5. Scattering diagrams contributing to the imaginary part mass operator $\Sigma(\epsilon)$ related to the band with a finite value of the Fermi velocity v_F . (a) The single line corresponds to a quasiparticle of this band, (b) the double line to the FC quasiparticle.

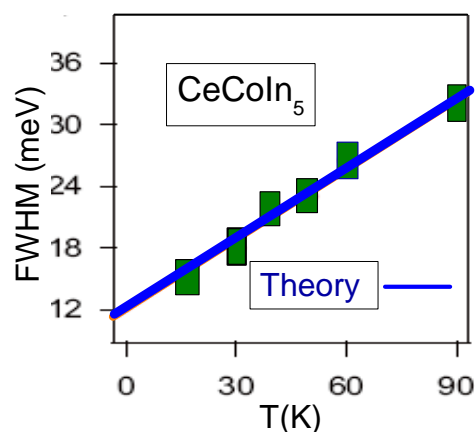


Figure 6. The temperature dependence of the full width at half maximum (FWHM) of the single-particle scattering rate of the main Kondo resonance [48] is shown by solid squares. The line represents the best fit: $\text{FWHM} = 11.8 + 2.69 T k_B$ meV, where k_B is Boltzmann's constant [48]. The solid line is our calculations [42].

5. T-Linear Resistivity and Planckian Limit

The exotic experimentally observed properties of various classes of HF compounds still remain largely unexplained due to the lack of a universal underlying physical mechanism. These properties are usually attributed to the so-called NFL behavior. The latter behavior is widely observed in heavy fermion (HF) metals, graphene, and high- T_c (HTSC) superconductors. Experimental data collected at many of these systems show that at $T = 0$, some of the excitation spectrum becomes dispersionless, which leads to flat bands; see [15–17,49,50]. The presence of flat bands indicates that the system is close to the topological fermion condensation quantum phase transition (FCQPT) [15–17,49], leading to the formation of flat bands given by Equation (4). Vivid experimental data on the linear temperature T dependence of resistivity $\rho(T) \propto T$, collected on HTSC, graphene, HF and ordinary metals, showed that the charge carrier scattering rate $1/\tau$ reaches the so-called universal Planck limit $1/(T\tau) = k_B/\hbar$ (k_B and $\hbar = h/2\pi$ are the Boltzmann and Planck constants, respectively) [30,31,49]. Note that this is above the Planck limit used to explain the universal scattering rate in so-called Planck metals [30,31,49], which can happen by chance because experimental manifestations in metals other than Planck can be just as well explained by more traditional physical mechanisms, such as those associated with phonon

contributions [50]. For example, ordinary metals exhibit a universal linear scattering rate at room and higher temperatures generated by well-known phonons, which are classical lattice excitations [30]. It is shown that, within the framework of the theory of fermion condensation, semiclassical physics is still applicable to describe the universal scattering rate $1/\tau$ experimentally observed in strongly correlated metals in their quantum critical region. This is due to the fact that the flat zones responsible for quantum criticality generate a transverse zero-sound mode, reminiscent of the phonon mode in solids with Debye temperature T_D [50,51]. At $T \geq T_D$, the mechanism of the linear temperature dependence of resistivity is the same in both ordinary and strongly correlated metals, and is represented by electron-phonon scattering. Consequently, it is the scattering of electrons on phonons at $T \geq T_D$ that gives almost material independence of the lifetime τ . It is expressed as $1/(\tau T) \sim k_B/\hbar$. Thus, the exciting experimental observations of the universal scattering rate related to linear-temperature resistivity of a large number of both strongly correlated Fermi systems and conventional metals can be explained [30,31,49–51]. The observed scattering rate is well explained by the appearance of flat bands formed by the topological FQCPT, rather than by the so-called Planck limit at which the supposed Planck scattering rate occurs. At low temperatures, the observed resistivity in their normal state for both HTSC and HF metals obeys the linear law given by Equation (10) with $\beta = 1$. On the other hand, at room temperature, the T -linear resistivity is exhibited by conventional metals, such as Al, Ag or Cu. In the case of a simple metal with a single pocket on the Fermi surface, the resistivity has the form $e^2 n \rho = p_F / (\tau v_F)$, where τ is the lifetime, e is the electronic charge, and n is the carrier concentration. The lifetime τ (or inverse scattering rate) of quasiparticles can be presented as

$$\frac{\hbar}{\tau} \simeq a_1 + \frac{k_B T}{a_2}, \quad (25)$$

and we obtain [50]

$$a_2 \frac{e^2 n \hbar}{p_F k_B} \frac{\partial \rho}{\partial T} = \frac{1}{v_F}, \quad (26)$$

where a_1 and a_2 are T -independent parameters. There are two challenging points for a theory. The first point is that experimental data confirm Equation (26) for both strongly correlated metals (HF metals and HTSC) and ordinary ones, provided that these demonstrate the linear T -dependence of their resistivity [30]; see Figure 7. The second point is, that under the application of a magnetic field, HF metals exhibit the LFL behavior; see Figure 3. For example, the HF metal CeRu₂Si₂ exhibits the LFL behavior under the application of a magnetic field as small as the magnetic field of the Earth [38]. Obviously, both of these two facts cannot be explained with the standard theories (see [35,52,53]) since the ordinary metals have nothing to do with the Planckian limit; moreover, such a small magnetic field cannot destroy the limit since the LFL behavior is not related to the limit.

The coefficient a_2 is always close to unity, $0.7 \leq a_2 \leq 2.7$, despite the huge difference in the absolute values of ρ , T and Fermi velocities v_F , which differ by two orders of magnitude [30]. As a result, it follows from Equation (25) that the T -linear scattering rate is of universal form $1/(\tau T) \sim k_B/\hbar$. This takes place in different systems displaying the T -linear dependence on the parameter entering Equation (26), $a_2 \simeq 1$ [30,50]. Indeed, such a dependence is demonstrated by ordinary metals at temperatures above the Debye one $T \geq T_D$, with an electron-phonon mechanism, as well as strongly correlated metals, that are supposed to be fundamentally different from ordinary ones, in which the linear dependence at their quantum criticality and temperatures of a few Kelvin are assumed to be due to electronic excitations rather than phonons [30]. As can be seen from Figure 7, this scaling relation spans two orders of magnitude in v_F , indicating the stability of the observed empirical law [30]. This behavior is explained within the framework of the PC theory since for both ordinary and strongly correlated metals, the scattering rate is determined by phonons [50,51]. In the case of ordinary metals at $T > T_D$ it is well known that the main contribution to the linear dependence of resistivity is made by phonons. On the other hand,

it is shown that semiclassical physics describes the T -linear dependence of the electrical resistance of strongly correlated metals at $T > T_D$ since the flat bands forming quantum criticality generate a transverse zero-sound mode with the Debye temperature T_D located inside the area of quantum criticality [50,51]. Consequently, the T -linear dependence is formed due to electron-phonon scattering both in ordinary metals and in strongly correlated ones. Thus, it is electron-phonon scattering that leads to the almost material independence of the lifetime τ , which is expressed as

$$\tau T \sim \frac{\hbar}{k_B}. \tag{27}$$

We emphasize that the Planck limit can arise by chance: it is extremely unlikely that it will occur in ordinary metals, which obviously cannot be recognized as a Planck limit with quantum criticality at high or low temperatures. The fact that we observe the same universal scattering rate behavior in microscopically different highly correlated compounds, such as HTSC, HF and common metals, suggests that some general theory is needed to provide a unified explanation for the above set of materials and their behavior. We confidently conclude that FC theory is a responsible approach to explaining the physics of strongly correlated Fermi systems.

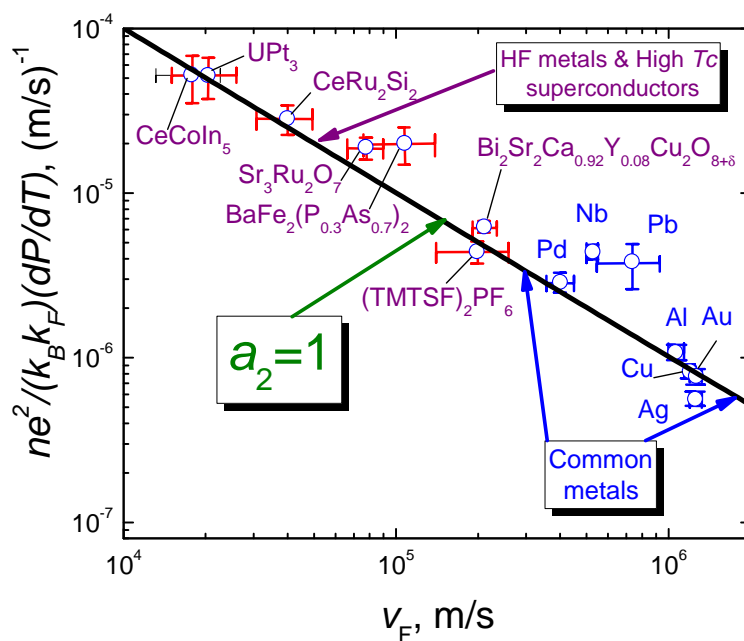


Figure 7. Scattering rates per kelvin vary greatly in correlated metals, such as HF, HTSC, organic and common metals [30]. All these metals have $\rho(T) \propto T$ and exhibit a change in Fermi velocities v_F by two orders of magnitude. The parameter $a_2 \simeq 1$ delivers the best fit, displayed by the solid line, and corresponds to the scattering rate $\tau T = \hbar / (2\pi k_B)$ with $\hbar = 2\pi\hbar$; see Equations (26) and (27). The region occupied by the conventional metals is highlighted by two (blue) arrows. The single (green) arrow shows the region of strongly correlated metals, including organic ones. Note that at low temperatures $T \ll T_D$, the scattering rate per kelvin of a conventional metal is orders of magnitude lower, and does not correspond to the Planckian limit. The area occupied by ordinary metals is highlighted by two (blue) arrows. The single (green) arrow shows the region of strongly correlated metals, including organic ones. We emphasize that at low temperatures $T \ll T_D$, the scattering rate per kelvin of an ordinary metal is orders of magnitude lower and is not in accordance with the Planck limit.

6. The Optical Conductivity of Heavy Fermion Metals

In this section, we use the FC theory to explain the NFL behavior of the optical conductivity based on experimental facts [32,33,54,55]. We show that ω/T -scaling be-

behavior of optical conductivity $\sigma_{opt}(\omega, T)$ is exhibited by HF compounds, where ω and T are the frequency and temperature, respectively. We show that because of the linear temperature dependence of the electrical resistivity $\rho(T) \propto T$, and at $\omega/T \geq 1$, the real part $\sigma_{opt}^R(\omega, T)$ of the optical conductivity $\sigma_{opt}(\omega, T)$ demonstrates the unusual power law behavior $\sigma_{opt}^R \propto \omega^{-1}$.

Modern condensed matter physics is vividly represented by the experimental discovery of flat bands [20,21,49], as they were predicted many years ago [7,15,16,18,23]. One can expect the existence of a general physical mechanism generated by the presence of flat bands and manifested in the universal scaling behavior of HF compounds. Indeed, HF compounds do exhibit universal scaling behavior and specific behavior caused by the presence of flat bands [7,9,10,22]. Within the framework of the fermion condensation theory, such a mechanism is represented by the topological FCQPT supporting quasiparticles, surviving the unlimited growth of the effective mass M^* , forming the non-Fermi liquid (NFL) behavior and generating flat bands [7,9,15,16,23]. The main goal of the quasiparticle interaction is to place the system at the topological FCQPT. As a result, the universal scaling behavior of HF metals can be explained, for it becomes independent of the interactions near the formation of flat bands. Thus, the universal scaling becomes independent of the interaction strength and its other properties for sufficiently large interactions [7,9]. However, it is important to explore new properties of HF compounds that are not directly determined by the effective mass M^* and cannot be explained within the framework of theories based on ordinary quantum phase transitions, the Kondo breakdown scenario, etc.; see, for example, [32,33,54,55]. For example, within the framework of the FC theory, the linear temperature dependence of electrical resistance $\rho(T) \propto T$ is explained, which is one of the main features of the behavior of the NFL [42,51], and can lead to a special behavior of optical conductivity exhibit HF metals. To analyze the optical conductivity $\sigma_{opt}(\omega, T)$, we use the Drude model (see [25])

$$\sigma_{opt}(\omega, T) = \sigma_0 \frac{1}{1 - i\omega\tau}. \quad (28)$$

Here, σ_0 reads

$$\sigma_0(T) = \frac{ne^2\tau(\omega, T)}{m} \Big|_{\omega=0}, \quad (29)$$

where the lifetime τ is given by Equation (24) [42,50,51]

$$\tau(\omega, T) = \frac{1}{a_0 + a_1T + a_2\omega}. \quad (30)$$

Here, $a_0 \propto \rho_0$, where ρ_0 is the residual resistivity; m , a_1 and a_2 are coefficients. The residual resistivity includes two contributions, $\rho_0 = \rho_{imp} + \rho_{FC}$, where ρ_{imp} comes from the impurities that hold a HF metal, and ρ_{FC} is formed by the FC state [42]; see Section 4. It is seen from Equations (29) and (30) that

$$\rho(T) = \rho_0 + \frac{m}{ne^2} a_1 T. \quad (31)$$

The NFL behavior of the lifetime τ is given by Equation (30), while in the LFL theory τ is given by [24,25,56]

$$\tau(\omega, T) = \frac{1}{a_0 + c_1 T^2 + c_2 \omega^2}, \quad (32)$$

where c_1 and c_2 are parameters and $a_0 \propto \rho_{imp}$ since FC is absent. As we will see, the NFL behavior of optical conductivity is determined by the NFL dependence of τ on both temperature T and frequency ω associated with the presence of FC; see Section 4. As a result, the scattering rate becomes $1/\tau \simeq a_0 + a_1 T$. This result is in good agreement with the experimental facts [47,48] presented in Figure 6. Thus, the FC theory successfully explains the behavior of both the scattering rate and the resistivity; see Equations (30) and (31) [42,50,51].

It is worth noting that in the case of HF metals and high- T_c superconductors, the scattering rate is a linear function of ω . Thus, we have to take into account the general expression for the optical conductivity since omitting the real part of the scattering rate leads to the Kramers-Kronig violation [57,58]. To restore the Kramers-Kronig relation, we employ the complex presentation of the scattering rate

$$\frac{1}{\tau(\omega)} \propto \left\{ \eta \omega \ln \left| \frac{\omega}{\omega_c} \right| + i(a_0 + a_2\omega) \right\}, \quad (33)$$

with η denoting the volume in momentum space occupied by the flat band, and ε_c being a characteristic constant [42,50]. Upon inserting Equation (33) into Equation (28), we obtain

$$\sigma_{opt} = \frac{ne^2}{m} \frac{1}{a_0 + a_1T + a_2\omega - i\omega(1 + \eta \ln \left| \frac{\omega}{\omega_c} \right|)}. \quad (34)$$

Taking into account that the logarithm $\eta \ln(\omega/\omega_c)$ on the right hand side of Equation (34) is a “slow” function of its variable, we approximate $1 + \eta \ln(\omega/\omega_c)$ by a constant c , as it is done in the next Section 6.1. Our calculations show that constant c is a good approximation for the logarithm.

6.1. Scaling Behavior of the Real Part σ_{opt}^R of the Optical Conductivity

Now, we are in position to consider the scaling behavior of $\sigma_{opt}(\omega, T)$. In the present context, the HF compounds are taken to represent strongly correlated Fermi systems as realized in HF metals and high- T_c superconductors. One can expect that HF compounds with their extremely diverse composition and microscopic structure would demonstrate very different thermodynamic, transport, and relaxation properties. Upon inserting Equation (29) into Equation (28), we obtain

$$\sigma_{opt}(\omega, T) = \frac{ne^2}{m} \frac{1}{a_0 + a_1T + a_2\omega - i\omega}. \quad (35)$$

To compare our theoretical results with the experimental facts, we subtract the residual resistivity (or conductivity), as it is done to the experimental facts [32,33,54,55], and obtain

$$\sigma_{opt}(\omega, T)T = \frac{b(1 + \omega/T) + ic\omega/T}{b^2(1 + \omega/T)^2 + (c\omega/T)^2}, \quad (36)$$

where b and c are parameters. It is seen from Equation (36) that $\sigma_{opt}(\omega, T)T$ depends on the only variable ω/T . It directly follows from Equation (36) that the real part σ_{opt}^R is given by:

$$\sigma_{opt}^R T = \frac{b(1 + \omega/T)}{b^2(1 + \omega/T)^2 + (c\omega/T)^2}. \quad (37)$$

Figures 8 and 9 display the scaling of the cuprate $\text{La}_{2-x}\text{Sr}_x\text{CuO}_4$ and the HF metal YbRh_2Si_2 in a wide range of the variable ω/T . At $\omega/T > 1$, the real part is proportional ω^{-1} , $\sigma_{opt}^R \propto \omega^{-1}$, and demonstrates the NFL behavior defined by the NFL behavior of τ ; see Equation (30). Figures 10 and 11 show the optical resistivity $1/\sigma_{opt}^R$ of $\text{La}_{2-x}\text{Sr}_x\text{CuO}_4$ and the HF metal YbRh_2Si_2 . It is seen that the resistivity is a linear function of the variable, as it should be, and seen from Figures 8 and 9.

The uniform scaling behavior seen in Figures 8 and 9 arises from the fact that HF compounds are located near a topological FCQPT that generates their uniform scaling behavior [7,9]. The emergence of the universal behavior, exhibited by very distinctive HF metals, supports the conclusion that HF metals represent a new state of matter [9,59]. Unlike the situation of a conventional quantum phase transition or the unconventional Kondo breakdown scenario, the scaling induced by topological FCQPT, as seen in Figures 8 and 9,

occurs up to high temperatures since the behavior of the NPL is determined by quasiparticles, and not by fluctuations or Kondo lattice effects [7,9].

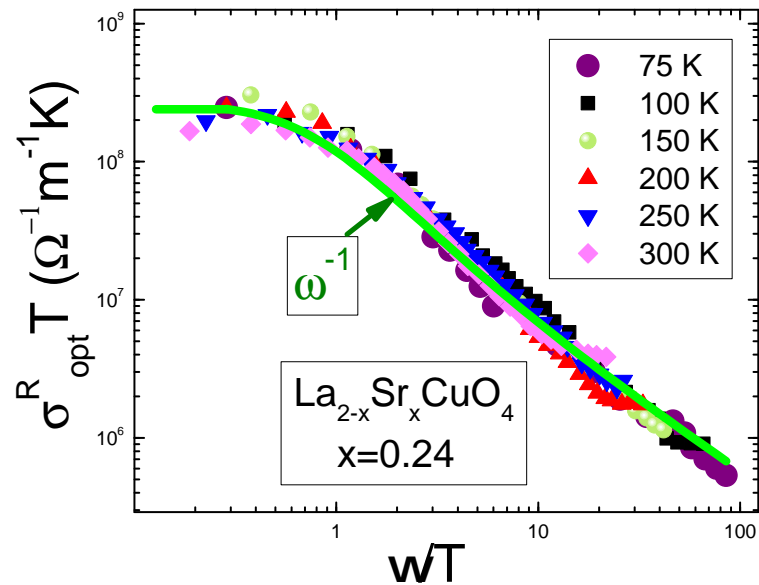


Figure 8. The ω/T scaling behavior of $\sigma_{opt}^R T$ of the cuprate $\text{La}_{2-x}\text{Sr}_x\text{CuO}_4$ [33]. At $\omega/T \geq 1$ $\sigma_{opt}^R \propto \omega^{-1}$, as it is shown by the arrow. The solid curve is our theory. Here and below, the theoretical real part $\sigma_{opt}^R(\omega, T)$ is given by Equation (37) with the parameters b and c chosen for the best description of the whole set of experimental data.

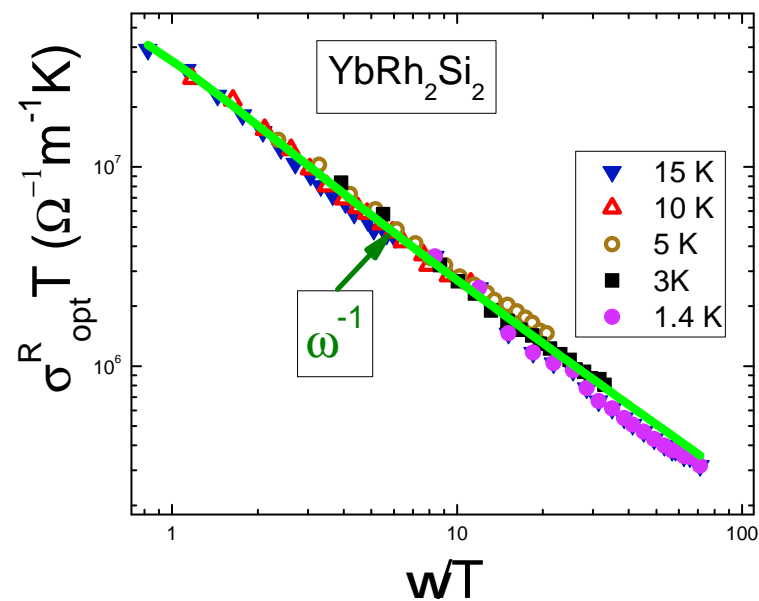


Figure 9. The ω/T scaling behavior of the real part $1/\sigma_{opt}^R T$ of the HF metal YbRh_2Si_2 [33]. At $\omega/T > 1$ $1/\sigma_{opt}^R \propto \omega^{-1}$ as it is shown by the arrow. The solid curve is our theory.

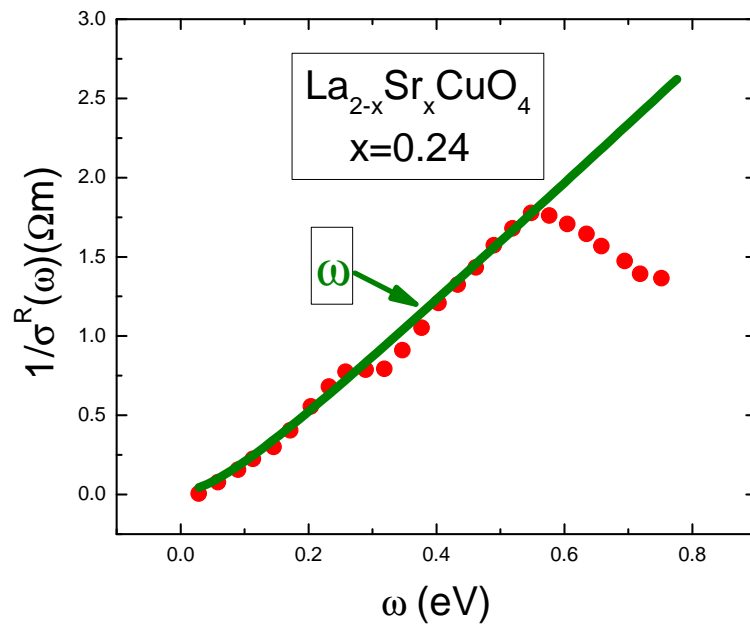


Figure 10. Optical resistivity $1/\sigma_{opt}^R(\omega, T)$ at 75 K of $\text{La}_{2-x}\text{Sr}_x\text{CuO}_4$ with $x = 0.24$, which is approximately linear in frequency up to 0.6 eV [33]. The solid line is our theory.

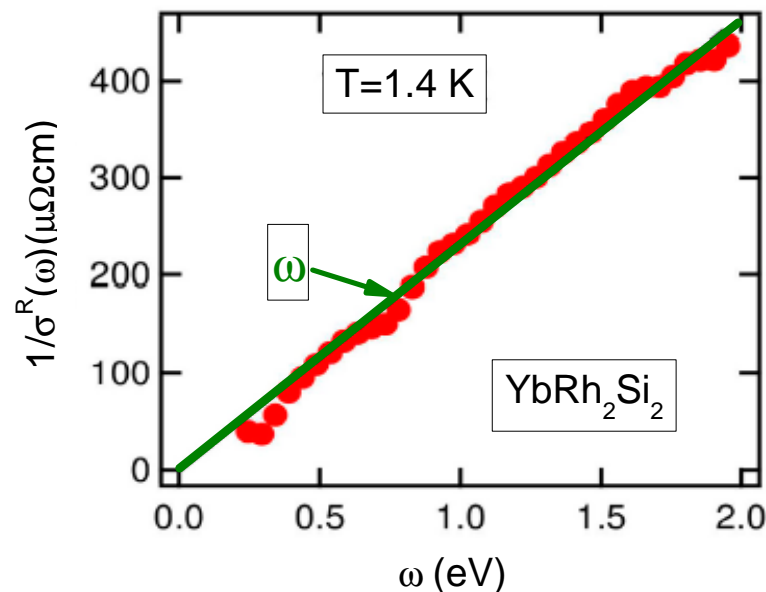


Figure 11. Optical resistivity $1/\sigma_{opt}^R(\omega, T)$ at 1.4 K of the HF metal YbRh_2Si_2 , which is approximately linear in frequency [33]. The solid line is our theory.

Violation of the Scaling Behavior

Now let us consider a possible violation of the observed scaling behavior of optical conductivity; see Figures 8 and 9. To understand the reasons for the violation, consider the schematic phase diagram of HF compounds. At $T = 0$, there is no crossover region, and the FC state is separated from the LFL region by the first-order phase transition [7] since the FC state is characterized by a special quantum topological number, being a new type of Fermi liquid [16,18]. At $T > 0$, it is not a phase transition that occurs but a crossover [7]. At elevated magnetic fields reaching $B \geq T$, the HF compound under consideration goes into the LFL state with $\rho(T) \propto T^2$. As a result, we assume that both Equation (32) and $\sigma_{opt}^R \propto \omega^{-2}$ become valid, while the NFL behavior of $\sigma_{opt}^R \propto \omega^{-1}$ vanishes. Such a behavior can be observed in measurements of the optical conductivity on the HF metal YbRh_2Si_2 at low temperatures under the application of magnetic field $B > B_{c0}$. Here, $B_{c0} \simeq 0.07$ T is the magnetic field that tunes YbRh_2Si_2 to its antiferromagnetic quantum critical point [60,61].

It is seen from Figure 12 that at $B > B_{c0}$ and $\mu_B B \geq k_B T$, YbRh₂Si₂ exhibits LFL behavior as it does at low temperatures in an antiferromagnetic state [61]. The HF metal YbRh₂Si₂ is one of the purest HF metals. Therefore, the regime of electron motion is ballistic. As a result, under the application of weak magnetic field B , one can observe a positive contribution $\delta \propto B^2$ to ρ_0 arising from the orbital motion of electrons induced by the Lorentz force. As seen in Figure 12, ρ_0 diminishes since the FC state is destroyed by the application of the magnetic field or by the antiferromagnetic state, and YbRh₂Si₂ demonstrates the LFL behavior with diminishing the magnetoresistance (see Figure 4), while the FC state itself creates the additional residual resistivity ρ_{FC} [22,42]. Thus, under the application of a magnetic field, the LFL behavior is restored, and the NFL one exhibited by optical conductivity is violated so that the scaling behavior following from Equations (30) and (35) vanishes. These measurement confirm both our theoretical consideration of the optical conductivity and the role of the magnetic field when studying the HF compounds [40]. We note that this role of the magnetic field is missed in the frameworks of marginal Fermi liquid, Kondo lattice, etc. [7,9].

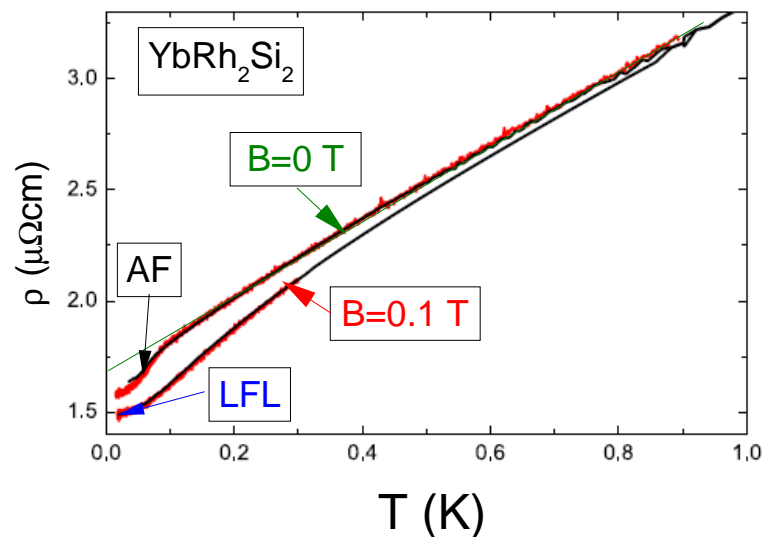


Figure 12. Temperature dependency of the electrical resistivities of YbRh₂Si₂ single crystals at magnetic fields $B = 0$ T and $B = 0.1$ T shown by the arrows [60]. The antiferromagnetic (AF) state at $B = 0$ T and the LFL state at $B = 0.1$ T are displayed by the arrows.

7. Conclusions

In our short review, we considered the transport properties of HF metals and high- T_c superconductors and showed that transport properties are defined by strong inter-particle interaction, leading to the topological FCQPT that forms flat bands, and makes the linear temperature resistivity $\rho(T) \propto T$. We analyzed the magnetoresistance and showed that under the application of a magnetic field, it becomes negative. We showed that the quasi-classical physics remains applicable to the description of the resistivity $\rho \propto T$ of strongly correlated metals due to the presence of a transverse zero-sound collective mode. Thus, in the region of T -linear resistance, electron-phonon scattering provides the lifetime τ of quasiparticles close to material independence, which is expressed approximately through the ratio of Planck's constant \hbar to the Boltzmann constant k_B , $T\tau \sim \hbar/k_B$. We showed that due to the NFL behavior of the resistivity $\rho(T) \propto T$, the real part σ_{opt}^R of the optical conductivity σ_{opt} exhibits a similar NFL behavior $\sigma_{opt}^R \propto \omega^{-1}$ rather than the well-known LFL relationship exhibited by ordinary metals $\sigma_{opt}^R \propto \omega^{-2}$. We predicted that under the application of a magnetic field, the real part of the optical conductivity behaves like $\sigma_{opt}^R \propto \omega^{-2}$ since the corresponding HF metal transits from the NFL behavior to the LFL one.

In summary, we showed that the fermion condensation theory provides a good description of the transport properties of various HF compounds, as our results are in good agreement with the experimental observations.

Author Contributions: V.R.S. and A.Z.M. designed the project and directed it with the help of M.V.Z., V.R.S. and A.Z.M. wrote the manuscript and all authors commented on it. The manuscript reflects the contributions of all authors. All authors have read and agreed to the published version of the manuscript.

Funding: This research received no external funding.

Institutional Review Board Statement: Not applicable.

Informed Consent Statement: Not applicable.

Data Availability Statement: Not applicable.

Acknowledgments: We thank V.A. Khodel for the fruitful discussions. This work was supported by U.S. DOE, Division of Chemical Sciences, Office of Basic Energy Sciences, Office of Energy Research, AFOSR.

Conflicts of Interest: The authors declare no conflict of interest.

References

1. Stewart, G.R. Non-Fermi-liquid behavior in *d*- and *f*-electron metals. *Rev. Mod. Phys.* **2001**, *73*, 797. [[CrossRef](#)]
2. Löhneysen, H.V.; Rosch, A.; Vojta, M.; Wölfle, P. Fermi-liquid instabilities at magnetic quantum phase transitions. *Rev. Mod. Phys.* **2007**, *79*, 1015. [[CrossRef](#)]
3. Gegenwart, P.; Si, Q.; Steglich, F. Quantum criticality in heavy-fermion metals. *Nat. Phys.* **2008**, *4*, 186. [[CrossRef](#)]
4. Sachdev, S. Quantum magnetism and criticality. *Nat. Phys.* **2008**, *4*, 173. [[CrossRef](#)]
5. Coleman, P.; Schofield, A.J. Quantum criticality. *Nature* **2005**, *433*, 226. [[CrossRef](#)]
6. Kadowaki, K.; Woods, S.B. Universal relationship of the resistivity and specific heat in heavy-Fermion compounds. *Solid State Commun.* **1986**, *58*, 507. [[CrossRef](#)]
7. Shaginyan, V.R.; Amusia, M.Y.; Msezane, A.Z.; Popov, K.G. Scaling behavior of heavy fermion metals. *Phys. Rep.* **2010**, *492*, 31. [[CrossRef](#)]
8. Shaginyan, V.R. Quasiparticles of strongly correlated Fermi liquids at high temperatures and in high magnetic fields. *Phys. At. Nucl.* **2011**, *74*, 1107. [[CrossRef](#)]
9. Amusia, M.Y.; Shaginyan, V.R. *Strongly Correlated Fermi Systems: A New State of Matter*; Springer Tracts in Modern Physics; Springer Nature: Cham, Switzerland, 2020; Volume 283.
10. Shaginyan, V.R.; Msezane, A.Z.; Japaridze, G.S. Peculiar Physics of Heavy-Fermion Metals: Theory versus Experiment. *Atoms* **2022**, *10*, 67. [[CrossRef](#)]
11. Coleman, P.; Pepin, C.; Si, Q.; Ramazashvili, R. How do Fermi liquids get heavy and die? *J. Phys. Condens. Matter* **2001**, *13*, R723. [[CrossRef](#)]
12. Coleman, P.; Pepin, C. What is the fate of the heavy electron at a quantum critical point? *C. Phys.* **2002**, *312–313*, 383. [[CrossRef](#)]
13. Khodel, V.A. Two scenarios of the quantum critical point. *JETP Lett.* **2007**, *86*, 721. [[CrossRef](#)]
14. Clark, J.W.; Khodel, V.A.; Zverev, M.V. Dissecting and testing collective and topological scenarios for quantum critical point. *Int. J. Mod. Phys. B* **2010**, *24*, 4901. [[CrossRef](#)]
15. Khodel, V.A.; Shaginyan, V.R. Superfluidity in systems with fermion condensate. *JETP Lett.* **1990**, *51*, 553.
16. Volovik, G.E. Quantum Phase Transitions from Topology in Momentum Space. *Lect. Notes Phys.* **2007**, *718*, 31.
17. Volovik, G.E. A new class of normal Fermi liquids. *JETP Lett.* **1991**, *53*, 222.
18. Volovik, G.E. Graphite, Graphene, and the Flat Band Superconductivity. *JETP Lett.* **2018**, *107*, 516. [[CrossRef](#)]
19. Volovik, G.E. From standard model of particle physics to room-temperature superconductivity. *Phys. Scr.* **2015**, *164*, 014014. [[CrossRef](#)]
20. Törmä, P.; Peotta, S.; Bernevig, B.A. Superconductivity, superfluidity and quantum geometry in twisted multilayer systems. *Nat. Rev. Phys.* **2022**, *4*, 528. [[CrossRef](#)]
21. Regnault, N.; Xu, Y.; Li, M.-R.; Ma, D.S.; Jovanovic, M. Catalogue of flat-band stoichiometric materials. *Nature* **2022**, *603*, 824. [[CrossRef](#)]
22. Khodel, V.A.; Clark, J.W.; Zverev, M.V. Topological disorder triggered by interaction-induced flattening of electron spectra in solids. *Phys. Rev. B* **2020**, *102*, 201108. [[CrossRef](#)]
23. Khodel, V.A.; Shaginyan, V.R.; Khodel, V.V. New approach in the microscopic Fermi systems theory. *Phys. Rep.* **1994**, *249*, 1. [[CrossRef](#)]
24. Lifshitz, E.M.; Pitaevskii, L. *Statistical Physics. Part 2*; Butterworth-Heinemann: Oxford, UK, 2002.
25. Pines, D.; Nozières, P. *Theory of Quantum Liquids*; Benjamin: New York, NY, USA, 1966.
26. Abrikosov, A.A.; Gor'kov, L.P.; Dzyaloshinski, I.E. *Methods of Quantum Field Theory in Statistical Physics*; Prentice-Hall: London, UK, 1963.
27. Paglione, J.; Tanatar, M.A.; Hawthorn, D.G.; Boaknin, E.; Hill, R.W.; Ronning, F.; Sutherland, M.; Taillefer, L.; Petrovic, C.; Canfield, P.C. Field-Induced Quantum Critical Point in CeCoIn₅. *Phys. Rev. Lett.* **2003**, *91*, 246405. [[CrossRef](#)] [[PubMed](#)]

28. Donath, J.G.; Steglich, F.; Bauer, E.D.; Sarrao, J.L.; Gegenwart, P. Dimensional Crossover of Quantum Critical Behavior in CeCoIn₅. *2008*, *100*, 136401. [[CrossRef](#)] [[PubMed](#)]
29. Gegenwart, P.; Westerkamp, T.; Krellner, C.; Brando, M.; Tokiwa, Y.; Geibel, C.; Steglich, F. Unconventional quantum criticality in YbRh₂Si₂. *Phys. B* **2008**, *403*, 1184. [[CrossRef](#)]
30. Bruin, J.A.N.; Sakai, H.; Perry, R.S.; Mackenzie, A.P. Similarity of Scattering Rates in Metals Showing *T*-Linear Resistivity. *Science* **2013**, *339*, 880. [[CrossRef](#)]
31. Legros, A.; Benhabib, S.; Tabis, W.; Laliberté, F.; Dion, M.; Lizaire, M.; Vignolle, B.; Vignolles, D.; Raffy, H.; Li, Z.Z.; et al. Universal *T*-linear resistivity and Planckian dissipation in overdoped cuprates. *Nat. Phys.* **2019**, *15*, 142. [[CrossRef](#)]
32. Homes, C.C.; Tu, J.J.; Li, J.; Gu, G.D.; Akrap, A. Optical conductivity of nodal metals. *Sci. Rep.* **2013**, *3*, 3446. [[CrossRef](#)]
33. Li, X.; Kono, J.; Si, Q.; Paschen, S. Is the optical conductivity of heavy fermion strange metals Planckian? *Front. Electron. Mater.* **2022**, *2*, 934691. [[CrossRef](#)]
34. Shaginyan, V.R. Density functional theory of fermion condensation. *Phys. Lett. A* **1998**, *249*, 237. [[CrossRef](#)]
35. Varma, C.M. Linear in temperature resistivity and associated mysteries including high temperature superconductivity. *Rev. Mod. Phys.* **2020**, *92*, 031001. [[CrossRef](#)]
36. Clark, J.W.; Khodel, V.A.; Zverev, M.V. Anomalous low-temperature behavior of strongly correlated Fermi systems. *Phys. Rev. B* **2005**, *71*, 012401. [[CrossRef](#)]
37. Hartmann, S.; Oeschler, N.; Krellner, C.; Geibel, C.; Steglich, F. Violation of critical universality at the antiferromagnetic phase transition of YbRh₂Si₂. *Phys. B* **2008**, *403*, 1254.
38. Takahashi, D.; Abe, S.; Mizuno, H.; Tayurskii, D.A.; Matsumoto, K.; Suzuki, H.; Ōnuki, Y. ac susceptibility and static magnetization measurements of CeRu₂Si₂ at small magnetic fields and ultralow temperatures. *Phys. Rev. B* **2003**, *67*, 180407. [[CrossRef](#)]
39. Shaginyan, V.R.; Msezane, A.Z.; Popov, K.G.; Stephanovich, V.A. Strongly Correlated Fermi-Systems: Magnetic-Field-Induced Reentrance of Fermi-Liquid Behavior and Spin-Lattice Relaxation Rates in YbCu_{5-x}Au_x. *Phys. Lett. A* **2009**, *373*, 3783. [[CrossRef](#)]
40. Shaginyan, V.R.; Msezane, A.Z.; Artamonov, S.A. Magnetic field as an important tool in exploring the strongly correlated Fermi systems and their particle-Hole and time reversal asymmetries. *Magnetism* **2023**, *3*, 180–203. [[CrossRef](#)]
41. Carretta, P.; Pasero, R.; Giovannini, M.; Baines, C. Magnetic-field-induced crossover from non-Fermi to Fermi liquid at the quantum critical point of YbCu_{5x}Au_x. *Phys. Rev. B* **2009**, *79*, 020401. [[CrossRef](#)]
42. Shaginyan, V.R.; Msezane, A.Z.; Popov, K.G.; Clark, J.W.; Zverev, M.V.; Khodel, V.A. Magnetic field dependence of the residual resistivity of the heavy-fermion metal CeCoIn₅. *Phys. Rev. B* **2012**, *86*, 085147. [[CrossRef](#)]
43. Nozières, P. Properties of Fermi liquids with a finite range interaction. *J. Phys. I France* **1992**, *2*, 443. [[CrossRef](#)]
44. Oeschler, N.; Gegenwart, P.; Lang, M.; Movshovich, R.; Sarrao, J.L.; Thompson, J.D.; Steglich, F. Uniaxial Pressure Effects on CeIrIn₅ and CeCoIn₅ Studied by Low-Temperature Thermal Expansion. *Phys. Rev. Lett.* **2003**, *91*, 076402. [[CrossRef](#)]
45. Ronning, F.; Capan, C.; Bauer, E.D.; Thompson, J.D.; Sarrao, J.L.; Movshovich, R. Pressure study of quantum criticality in CeCoIn₅. *Phys. Rev. B* **2006**, *73*, 064519. [[CrossRef](#)]
46. Bianchi, A.; Movshovich, R.; Oeschler, N.; Gegenwart, P.; Steglich, F.; Thompson, J.D.; Pagliuso, P.G.; Sarrao, J.L. First-Order Superconducting Phase Transition in CeCoIn₅. *Phys. Rev. Lett.* **2002**, *89*, 137002. [[CrossRef](#)] [[PubMed](#)]
47. Aynajian, P.; Neto, E.; Gyenis, A.; Baumbach, R.E.; Thompson, J.D. Visualizing heavy fermions emerging in a quantum critical Kondo lattice. *Nature* **2012**, *486*, 201. [[CrossRef](#)] [[PubMed](#)]
48. Chen, Q.Y.; Xu, D.F.; Niu, X.H.; Jiang, J.; Peng, R. Direct observation of how the heavy-fermion state develops in CeCoIn₅. *Phys. Rev. B* **2017**, *96*, 045107. [[CrossRef](#)]
49. Cao, V.; Fatemi, S.; Fang, K.; Watanabe, K. Unconventional superconductivity in magic-angle graphene superlattices. *Nature* **2018**, *556*, 43. [[CrossRef](#)]
50. Shaginyan, V.R.; Popov, K.G.; Khodel, V.A. Quasiclassical physics and *T*-linear resistivity in both strongly correlated and ordinary metals. *Phys. Rev. B* **2013**, *88*, 115103. [[CrossRef](#)]
51. Khodel, V.A.; Clark, J.W.; Shaginyan, V.R.; Zverev, M.V. Second wind of the Dulong-Petit Law at a quantum critical point. *JETP Lett.* **2010**, *92*, 532. [[CrossRef](#)]
52. Patel, A.A.; Sachdev, S. Theory of a Planckian Metal. *Phys. Rev. Lett.* **2019**, *123*, 066601. [[CrossRef](#)]
53. Volovik, G.E. Flat Band and Planckian Metal. *JETP Lett.* **2019**, *110*, 352. [[CrossRef](#)]
54. Prochaska, L.; Li, X.; MacFarland, D.C.; Andrews, A.M.; Bonta, M.; Bianco, E.F.; Yazdi, S.; Schrenk, W.; Detz, H.; Limbeck, A.; et al. Singular charge fluctuations at a magnetic quantum critical point. *Science* **2020**, *367*, 285. [[CrossRef](#)]
55. Michon, B.; Berthod, C.; Rischau, C.W.; Ataei, A.; Chen, L.; Komiyama, S.; Ono, S.; Taillefer, L.; van der Marel, D.; Georges, A. Reconciling scaling of the optical conductivity of cuprate superconductors with Planckian resistivity and specific heat. *Nat. Commun.* **2023**, *14*, 3033. [[CrossRef](#)] [[PubMed](#)]
56. Gurzhi, R.N. Mutual Electron Correlations in Metal Optics. *Sov. Phys. JETP* **1959**, *8*, 673.
57. Götze, W.; Wölfle, P. Homogeneous Dynamical Conductivity of Simple Metals. *Phys. Rev.* **1972**, *6*, 1226. [[CrossRef](#)]
58. Littlewood, P.B.; Varma, C.M. Phenomenology of the normal and superconducting states of a marginal Fermi liquid. *J. Appl. Phys.* **1991**, *69*, 4979. [[CrossRef](#)]
59. Shaginyan, V.R.; Stephanovich, V.A.; Msezane, A.Z.; Schuck, P.; Clark, J.W.; Amusia, M.Y.; Japaridze, G.S.; Popov, K.G.; Kirichenko, E.V. New State of Matter: Heavy Fermion Systems, Quantum Spin Liquids, Quasicrystals, Cold Gases, and High-Temperature Superconductors. *J. Low Temp. Phys.* **2017**, *189*, 410. [[CrossRef](#)]

60. Pfau, H.; Hartmann, S.; Stockert, U.; Sun, P.; Lausberg, S.; Brando, M.; Friedemann, S.; Krellner, C.; Geibel, C.; Wirth, S.; et al. Thermal and electrical transport across a magnetic quantum critical point. *Nature* **2012**, *484*, 493. [[CrossRef](#)]
61. Gegenwart, P.; Custers, J.; Geibel, C.; Neumaier, K.; Tayama, T.; Tenya, K.; Trovarelli, O.; Steglich, F. Magnetic-Field Induced Quantum Critical Point in YbRh₂Si₂. *Phys. Rev. Lett.* **2002**, *89*, 056402. [[CrossRef](#)]

Disclaimer/Publisher's Note: The statements, opinions and data contained in all publications are solely those of the individual author(s) and contributor(s) and not of MDPI and/or the editor(s). MDPI and/or the editor(s) disclaim responsibility for any injury to people or property resulting from any ideas, methods, instructions or products referred to in the content.